Verdú, S.; Ruiz Rico, M.; Barat Baviera, JM.; Grau Meló, R. (2021). Evaluation of the influence of food intake on the incorporation and excretion kinetics of mesoporous silica particles in C.elegans. Chemico-Biological Interactions. 334:1-8. https://doi.org/10.1016/j.cbi.2020.109363

Evaluation of the influence of food intake on the incorporation and excretion kinetics of mesoporous silica particles in *C.elegans*

Samuel Verdú, María Ruiz-Rico, José M. Barat, Raúl Grau

Departamento de Tecnología de Alimentos. Universitat Politècnica de València, Spain

*Author for correspondence: Samuel Verdú

Address: Edificio 8E - Acceso F – Planta 0

Ciudad Politécnica de la Innovación

Universitat Politècnica de València

Camino de Vera, s/n

46022 VALENCIA – SPAIN

E-mail: saveram@upvnet.upv.es

Abstract

The effect of the presence of food on the incorporation and excretion of silica particles was studied in this work using the biological model *Caenorhabditis elegans* and image analysis techniques. The experiment was based on two 24-hour phases: exposure and depuration. During exposure, nematodes were maintained for 24 h in liquid medium with silica particles, but some with and others without food. During depuration, nematodes were transferred to medium without particles. Nematodes were analysed by an image analysis in both phases to quantify the properties of particle distributions in nematodes´ bodies with time. No differences were found in the proportion of nematodes carrying particles in the exposure phase when food was present. However in the depuration phase, lack of food generated a high proportion of particle carriers. Particle distribution properties were also similar in the exposure phase. Nevertheless, lack of food produced particle accumulation due to decelerated excretion because digestive tube relaxed under these conditions. Thus after the depuration phase, lack of food led particles to persist in digestive tubes. According to these results, intake of silica particles had no retention effects when a food flux was provided, but particles were not easily excreted when the food flux was interrupted.

Keywords: silica particles, uptake kinetics, digestive tube, image analysis, *C.elegans*

1. Introduction

Microparticles (*MPs*) are defined as materials of sizes >100 nm (Nowack and Bucheli, 2007). *MPs* possess unique size-dependent physico-chemical properties that serve for many socio-economic and industrial benefits, ranging from pharmaceuticals to athletic gear (Maurer-Jones et al., 2013). These materials have unique physico-chemical properties that can lead to new technological applications with potential usefulness for sensors, catalysis, etc. Given inadequate traditional food conservation systems and a rise in antibiotic-resistant bacteria and fungal strains, new strategies to prevent food spoilage and contamination are being researched with such materials. Immobilisation of compounds on solid matrices offers higher potential in relation to the above-mentioned aim. This process increases antimicrobial capacity with a small amount of compound compared to its free version. Recently, our research group reported a new antimicrobial system based on the covalent immobilisation of plant essential oils on silica supports to preserve and enhance their antimicrobial effect against pathogen and spoilage microorganisms in both *in vitro* and *in situ* studies (Fuentes et al., 2020; Ribes et al., 2019; Verdú et al., 2020)

The main properties governing *MPs* behaviour are surface area, particle size, degree of agglomeration, surface charge, particle morphology, surface coating, particle composition and crystalline structure (Turan et al., 2019). Those properties and chemical composition are usually well characterised and controlled, but the interaction of *MPs* with biological fluids and tissues need to be studied in-depth. Therefore, performing well-planned experiments *in vitro* and *in vivo* with simple animals is fundamental to reduce the number of sample categories before screening them in high-order animals. Therefore, assays providing useful biological information at lower costs during *MPs* development are very much in demand. These studies suggest that understanding the effect on *in vivo* kinetics and biocompatibility is essential for improving the performance of new applications for more research fields.

Caenorhabditis elegans (*C. elegans*) are non-parasitic nematodes used in toxicity bioassays because they provide numerous advantages in both time and cost terms. Some of these advantages are growing large quantities of these organisms in Petri dishes with a rapid life cycle (3 days),

and transparency to allow transgenic proteins to be fused to fluorescent markers to become visible in live animals in *in vivo* experiments. Although they have a much simpler structure than higher mammals like humans, this animal model possesses a similar number of genes (worms 20,000 genes, humans 23,000 genes) (Gonzalez-Moragas et al., 2015). They also possess similarities in organs and biological functions, such as epithelial, digestive, excretory and neuronal systems (Breimann et al., 2019; Ruszkiewicz et al., 2018), which allows food intake and excretion processes to be studied under different conditions and how they are affected by external conditions. These studies could be carried out with protocols that combining exposure-depuration phases, where nematodes are studied during an exposure to a given compound, from which they are trespassed to a clean medium with the aim of modelling the elimination kinetics.

Assessing the interaction between *MPs* and *C. elegans* has provided information about *in vivo* behaviour in a multicellular organism of some particles to evaluate their fate and toxicity. Some examples include studying the toxicity of silver particles on nematodes´ oxidative stress and DNA damage (Ahn et al., 2014), the role of charge in the toxicity of polymer-coated cerium oxide nanomaterials (Arndt et al., 2017), the toxicity of hydroxylated fullerene particles (Cha et al., 2012), the properties of gold particles (Gonzalez-Moragas et al., 2017a), the toxicogenomics of iron oxide particles (Gonzalez-Moragas et al., 2017b), etc.

This work focused on studying the influence of food intake on the interaction of mesoporous silica particles with the tissues of the nematode *C.elegans* by modelling the incorporation and excretion kinetics using image analysis techniques.

2. Material and Methods

2.1. Experiment procedure

The experiment was based on controlling the presence/absence of food in two different phases: exposure and depuration. The exposure phase consisted in exposing nematodes to MCM41-

particles (Mobil Composition of Matter No. 41) for 24 h. The depuration phase involved putting nematodes into medium without particles for the next 24 h. This procedure was common for both groups of nematodes. The two groups were divided by differentiating feed status. Group-A (absence) was the group without food in both phases, while group-P (presence) was provided with *E.coli* OP50 throughout the assay. While the assay was underway, pictures of nematodes were taken at different times to be transformed and analysed by imaging analysis procedures to acquire information about the features of particles in nematodes with time. Particle features were studied based on the parameters offering information about particle distribution start and end points, as well as length. Particle area was also calculated with time to study the effect of feed status on particle aggregation in the digestive tubes of nematodes.

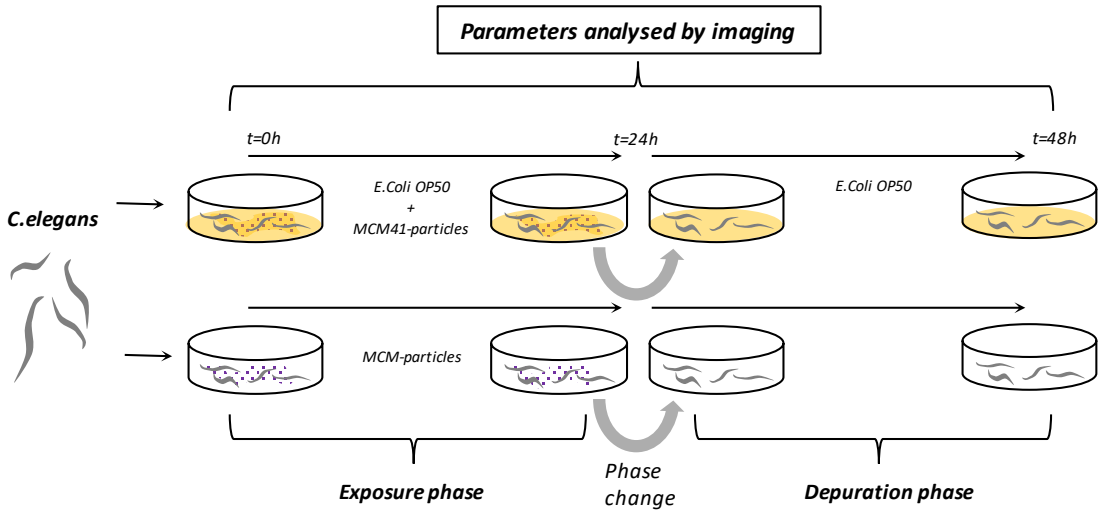

Figure 1. Experiment scheme

2.2. Particle synthesis and characterisation

2.2.1 Reagents

Tetraethylorthosilicate (TEOS), N-cetyltrimethylammonium bromide (CTABr), NaOH, triethanolamine (TEAH3), (3-Aminopropyl)triethoxysilane (APTES) and rhodamine B isothiocyanate were provided by Sigma-Aldrich (Madrid, Spain). Ethanol was purchased from Scharlab (Barcelona, Spain).

2.2.2. Synthesis of MCM-41 particles

Bare microsized mesoporous silica particles were synthesised and characterised by standard procedures (Ruiz-Rico et al., 2017). MCM-41 particles were synthesised from TEOS using CTABr as a structural directing agent, followed by template removal by calcination (Ruiz-Rico et al., 2016). For the synthesis, triethanolamine (TEAH3) (25.06 g) was mixed with a NaOH (0.98 g) solution in deionised water (2 mL). The mixture was heated to 120ºC. Next the solution temperature was adjusted to 70ºC. TEOS (11 mL) was added and heated to 120ºC. The solution temperature was adjusted to 118ºC and CTABr (4.68 g) was slowly added. The reaction mixture was cooled to 70ºC and deionised water (80 mL) was added with vigorous stirring. The white suspension was aged at 100ºC for 24 h. The obtained powder was isolated by filtration, and washed with ethanol and water. The solid was firstly dried at 70ºC and then calcined at 550ºC in an oxidant atmosphere for 5 h.

2.2.3 Marking MCM-41 particles

The MCM-41 microparticles were labelled with rhodamine B isothiocyanate to detect them throughout the nematode body by fluorescence microscopy. Firstly, the solid surface was modified with APTES. For this purpose, 1 g of particles was suspended in ethanol (30 mL) and 0.19 mL of APTES (0.8 mmol) were added. The mixture was stirred for 1 h, and then the suspension was centrifuged and washed with ethanol. The obtained solid was suspended in ethanol and reacted with rhodamine B isothiocyanate for 20 h. The mixture was centrifuged and washed with abundant deionised water. Finally, the solid was dried for 12 h at 37ºC to obtain the labelled material.

2.2.4 Characterisation of synthesised particles

Both the bare and labelled silica particles were characterised to establish their zeta potential, particle size distribution and degree of labelling. The zeta potential was analysed by Zetasizer Nano ZS (Malvern Instruments, UK). The silica particles were dispersed in "K-medium" liquid medium (1 mg/mL) and sonicated for 2 min to avoid aggregation. The zeta potential was calculated by applying the Smoluchowski model using the obtained results from the particle mobility analysis. The zeta potential was reported as the average of three independent analysis. Particle size distribution was determined by a Malvern Mastersizer 2000 device (Malvern Instruments, UK). Samples were conditioned by dispersing in water and sonicated for 2 min. The light scatter data was accumulated for 10 s for each, which were measured in triplicate. The degree of functionalisation was determined by a thermo-gravimetric analysis (TGA). A TGA was carried out on a TGA/SDTA 851e Mettler Toledo balance (Mettler Toledo Inc., Schwarzenbach, Switzerland) in an oxidant atmosphere (air 80 mL/min) with a heating programme consisting of heating steps at 5ºC per minute from 25ºC to 1,000ºC.

2.3. *C.elegans* preparation

Wild-type *Cahenorabditis elegans* Bristol strain N2 was employed as the biological model. The population of nematodes were reproduced on nematode growth medium (NGM) plates seeded with *E. coli* OP50 at 20ºC (Brenner, 1974). Animals was synchronised by the standard bleach method (Stiernagle, 2006). The age-synchronised L4 individuals were used to perform the experiment.

2.4. Exposure procedure

Assays were carried out in the "K-medium" liquid medium (32 mM of KCl, 51 mM of NaCl) following the protocols of Zhou et al., (2016). The concentration of particles in the exposure phase was 6 µg/mL. *E.coli* OP50 was used as food for group-P. Exposure was done in 3.4 mL-well plates (Corning® 3738 Costar® 24-Well Flat Bottom) at 20ºC in an incubator. Fifty nematodes were exposed per experiment, which were done in triplicate.

2.5. Image acquisition

Image acquisition was done periodically in both assay phases at 0, 3, 6, 15, 24, 25, 27, 30, 40 and 48 h. Nematodes were extracted from medium and introduced into a drop of 0.25M sodium azide, employed as anaesthesia. Drops were placed on a poly-l-lysine-covered slide (Sigma-Aldrich, Madrid, Spain) to be covered with a coverslip. Preparation was evaluated by a Motic BA310E trinocular microscope equipped with an Epi-Led module, an MB barrier filter and a Moticam 3+ camera. Images from the light field and fluorescence were taken to visualise the entire nematode anatomy and to quantify the particle distribution properties with an image analysis technique. Images were combined to show some examples of the position of particles in nematodes.

2.6. Image processing

Fluorescent images were processed to quantify the properties of particle distributions in nematodes at each sampling time during the assay. Particles exhibited an orange tone under the fluorescent conditions because they were stained with rhodamine (Figure 2A). This property was used to isolate the pixels containing particles (equivalence of 1,666 pixels/mm). Segmentation was done based on the RGB parameters of the pixels with particles and by extracting the rest of the image. The result was binarised images (White-Black), where particles were represented as a white area (Figure 2B). The analysed properties of that area were:

- *% particle carriers*: proportion of nematodes with detected pixels corresponding to particles. Expressed as % of nematodes.
- *A*: distance from the head to the start point of particle distribution in nematodes. Expressed as number of pixels
- *B*: distance from the head to the end point of particle distribution in nematodes. Expressed as number of pixels
- *L*: difference between B and A. Expressed as number of pixels

- P_A: particle area is the area of pixels containing the particle aggregates. Expressed as number of pixels.

Fifty images of nematodes were analysed in triplicate.

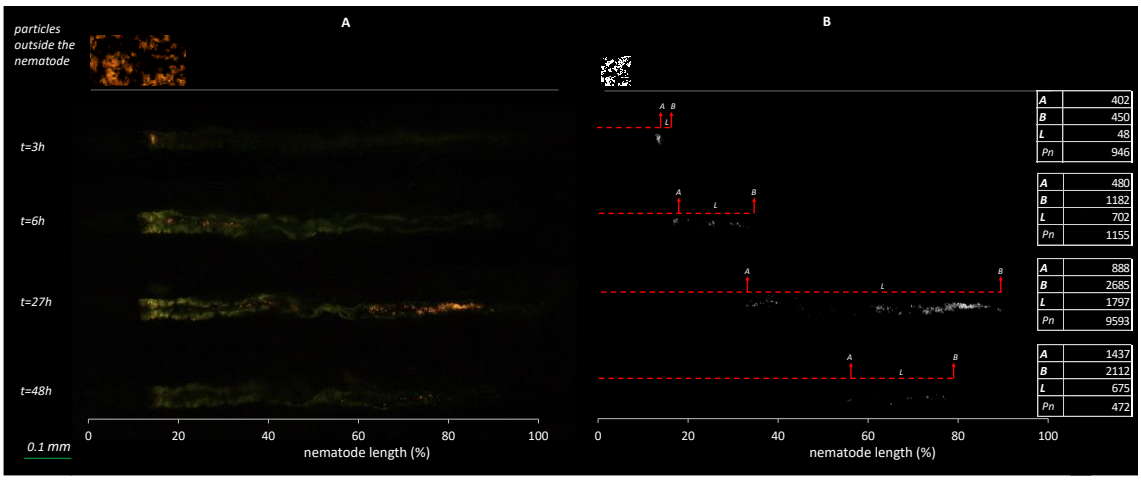

Figure 2. Image processing and data extraction of particle distributions. A: fluorescence image of MCM41-particles outside and inside nematodes at different assay times. B: images of the isolated particles after processing by image segmentation. The red line represents nematode length from the head to the end of particle distribution, where A: start of MCM41-particle distribution; B: end of MCM41-particle distribution; L = B-A; Pn: number of particles.

2.7. Statistical analysis

The data from the image analysis of particle distributions were analysed by time series to know the kinetics of the extracted parameters in assay phases.

3. Results and Discussion

3.1. Materials characterisation

Table 1 shows the results of the particle size distribution, zeta potential and organic matter content of the bare and functionalised particles. The bare and labelled MCM-41 particles displayed a size distribution within the microscale size range in accordance with the *d0.5* values.

Functionalisation efficiency was evaluated by the zeta potential determinations and TGA analysis. The bare MCM-41 particles exhibited negative zeta potential values of ca. -30 mV due to the presence of silanol groups on the surface of the support. In contrast, the Rho-labelled particles

presented a positive zeta potential because of the grafting of the Rho-alkoxysilane derivative. Finally, the content of organic matter attached to MCM-41 came to 0.06 g/g SiO_2, which confirmed that functionalisation had been successful.

Table 1. Characterisation parameters of the bare and labelled MCM-41 particles: particle size distribution ($d_{0.5}$), zeta potential and content (α) in grams of rhodamine B isothiocyanate per gram of SiO_2.

	Size $d_{0.5}$ (µm)	Zeta potential (mV)	α_{Rho} (g/g SiO_2)
Bare	0.711±0.021	-34.0±1.7	-
Rho-labelled	0.680±0.042	17.4±2.7	0.06

3.2. Evolution of the presence of particles in the population

The incorporation of particles into the population was evaluated by scoring nematodes with particles in digestive tubes with time (% particle carriers). The results expressed as percentages are found in Figure 3. The evolution of the % of particle carriers showed no differences in the exposure phase (first 24 h). The presence of food had no effect on the incorporation of particles. The population from both groups presented the highest slope between 0-3, where 75% particle carriers were reached. From this point, the velocity of incorporation was reduced to 24 h by increasing the % of particle carriers up to 95%.

After exposure, differences appeared for the groups' kinetics. Particle carriers were maintained up to 98% until 27 h, from which time the values lowered until the assay ended. In this case, the velocity of group-P was the highest. This group reached less than 10% particle carriers at 40 h and 0% at 48 h. Moreover, group-A dropped to around 75% particle carriers for 48 h.

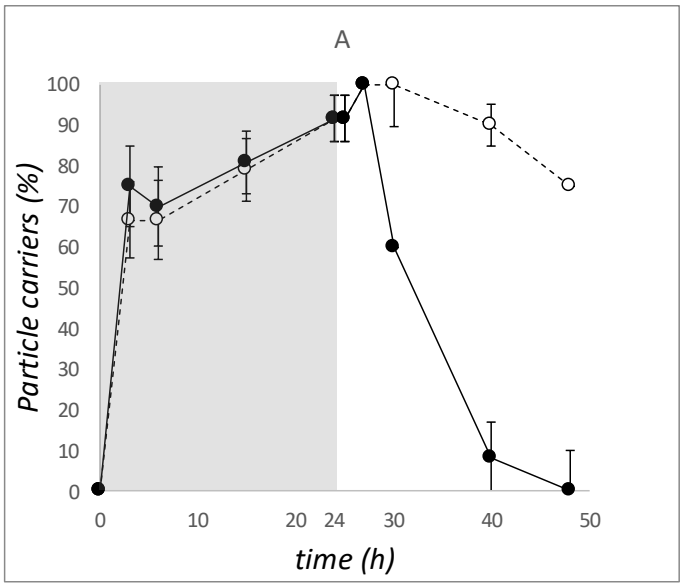

Figure 3. Evolution of the nematode population with MCM-particles in the digestive system during the assay. ● group-P; ○ group-A. The grey zone marks the exposure phase and the white zone denotes the depuration phase. Bars mark standard deviation.

In this case, the presence of food strongly influenced the excretion of particles from nematodes' digestive tubes. Figure 4A and 4B are examples of nematodes from group-P and -A, respectively, after 24 h of exposure to show that effect. The nematode population from group-P (Figure 4A) showed particles along the entire digestive tube, while the group-A nematodes (Figure 4B) revealed that particles accumulated after the pharynx in the first digestive tube zone. So although different distributions in nematodes´ digestive tubes were observed, the similar evolution of particle carriers in the exposure phase evidenced a common pumping stimulus produced by particles and *E.coli*. This observation contrasts with other results provided by Pluskota et al. (2009), who reported that the presence of food favoured the uptake of particles when impregnated in the *E.coli* law because it could simultaneously incorporate both components.

Figure 4. Detecting particles in *C.elegans* during the assay. A: image of particles along the digestive tube of a nematode from group-P after 18 h of exposure; B: image of particles in the principle digestive tube of a nematode from group-A after 18 h of exposure; C: particles retained in the pharynx and the digestive tube of nematodes from group-A at the end of the depuration phase. Arrows mark particle accumulations.

The same score of particles carriers after 24 h of exposure between both groups could reveal the stimulating effect of particles themselves. This effect could be attributed to *C.elegans* pharyngeal pumping, a mechanism by which nematodes introduce food into their organism, which constantly works like simple food filters through the pharynx (Gonzalez-Moragas et al., 2015). Nematodes are filter feeders, in which pumping generates contraction cycles to suck in solids and liquid. During relaxation, liquid phases are ejected to the medium and solids, normally bacteria, are retained in the pharynx and transported to the intestine (Altun et al., 2007). Thus our results showed how synthesised MCM-particles could enter nematodes via this mechanism without food being present.

The depuration phase evidenced the isolated effect of the presence of food given the rapid expulsion of particles from the group-P nematodes. Group-A presented high scores of particle carriers. It was because lack of food brought about the observed accumulations due to intestinal relaxation, which slowed down particle expulsion velocity. In *C. elegans*, defecation is slow when food is scarce, and can even be inhibited as feeding ceases to be resumed only when food becomes available again (Donald L Riddle, 1997). When the group-A nematodes had no stimuli, particles reduced the expulsion velocity by more than half, and the residence time prolonged as did the % particle carriers. Figure 4C shows the accumulated particles after the 24-hour depuration phase located in the pharynx zone of the group-A nematodes. This revealed how no differences appeared

for the uptake of particles between groups. However, differences were found for their distribution, which means that studying particle distribution during assays is necessary.

3.3. Position and distribution of particles

Particles were tracked in nematodes by an image analysis to know where and how particles were distributed at each sampling time. Parameters *A, B* and *L* were used for this purpose. Figure 5A shows the evolution of parameter *A* (particle distribution start point from the head) with time. The exposure phase showed a similar evolution for both groups. This behaviour was related to the fact that particles were continuously available in the exposure phase. With the presence of food/particles, nematodes incorporated particles all the time and, therefore, particles were found at the beginning of the digestive tube at any time. This zone comes after the pharynx. The pharynx is sited at around 10-15% of nematode length. In that % of nematode length, particles were found throughout the exposure phase. However, when nematodes started the depuration phase, different behaviours were observed for each group. Group-P showed ascendant evolution with time in which A reached 100% nematode length before expulsion. Conversely, group-A presented particles with a nematode length of around 10%, as in the exposure phase. These observations support what is mentioned above; "without food, excretion velocity and the peristaltic stimulus slowed down". This effect was evidenced by studying the extension of particle distribution L into nematode and B (particle distribution end point from the head). Figure 5B shows the evolution of B with time, in which case both groups showed similar evolution in the exposure phase. Both groups displayed an increased position of B with a similar slope, but group-A presented a shorter nematode length of around 15% than group-P. The positions at 24 h were 35% and 50% nematode length for group-A and -P, respectively. As with *A, B* intensely increased from 24 h for group-P, while group-A presented an almost constant state. These differences observed in particle distribution evolution generated a different extension of material along digestive tubes, principally in group-P, which could be measured by parameter *L* (Figure 5C).

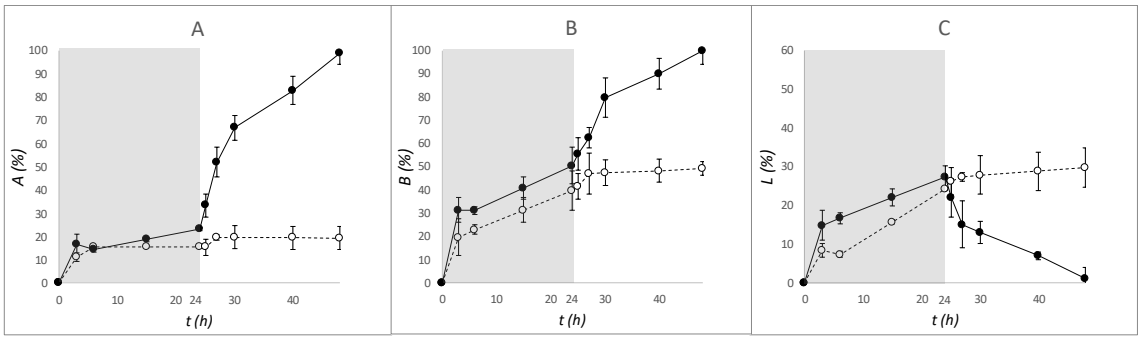

Figure 5. Evolution of the position parameters of the MCM-particles in the digestive system during the assay. A: evolution of the start of distribution in nematode *A* during the assay; B: evolution of the end of distribution in nematode *B* during the assay; C: evolution of particle distribution extension *L* in nematodes during the assay. ● group-P; ○ group-A. The grey zone marks the exposure phase, and the white zone denotes the depuration phase. Bars mark standard deviation.

For group-P, *L* increased by around 30% at 24 h of exposure, from which time this value inversed until it reached to 0% at 48 h. No particles were detected in digestive tubes when the assay ended. In group-A, *L* increased in the exposure phase to 30%, but slightly increased in the depuration phase. As *A* had minimum modifications for this group throughout the assay, an increase in particle extension throughout the nematode digestive system was observed, represented by a slight increase in *L* in the depuration phase (Figure 5C).

Differences in behaviours were caused by the presence of food increasing particle circulation velocity. Then when nematodes started the depuration phase (particles were absent), *A* advanced and *L* lowered to almost 0% at 48 h. These results agree with those reported by Däwlätşina et al. (2013), who studied magnetic and silver particles, and described how feeding *E. coli* with particles over time also resulted in uniform distributions of particles in the body than when feeding worms only particles. Thus the presence of food was insignificant in the particles position during exposure, but residence time was directly affected by absence of food.

3.4. Characterising particle aggregates

After learning how much of the population had incorporated particles and their location in the organism, the image analysis focused on quantifying particle aggregates (P_A). The results express the amount of pixels containing the particle cumulus quantified along the distribution take took place during residence in nematodes. Figure 6 shows the P_A results. Both groups presented the same increase in area in the exposure phase, which remained constant until the end of the phase. This fact agrees with the evolution of position parameters *A* and *B* and, in this case, it seemed that no different amounts of particles were ingested in the exposure phase. The non-effect of the presence of food was shown in that phase. Moreover, the groups followed different evolutions when the depuration phase started. Group-A displayed increased P_A until 40 h at the most. Conversely, group-P went from t=27h to the end and reached P_A=0 at 48 h; that is to say, no detected particles.

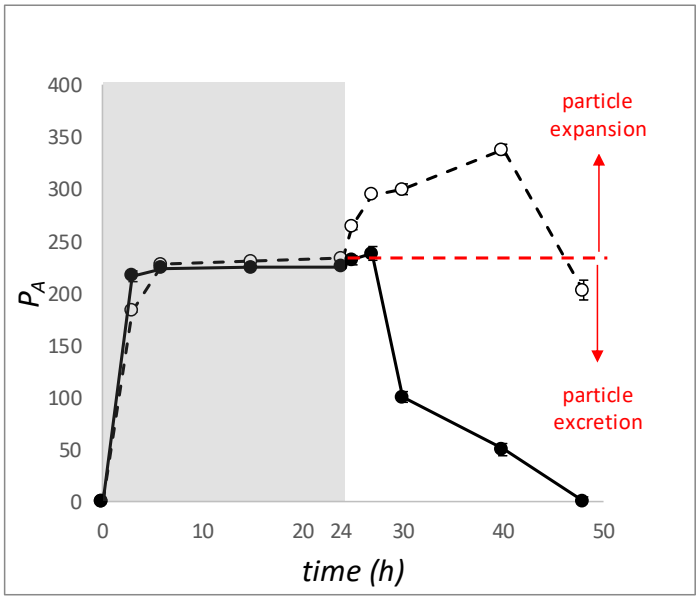

Figure 6. Evolution of the aggregates of the MCM-particles in the digestive system during the assay. ● group-P; ○ group-A; P_A: particle aggregates area (pixels). The grey zone marks the exposure phase and white zone denotes the depuration phase. Bars mark standard deviation.

The observed results suggest an increased particle content in the depuration phase for group-A, but this is impossible because particles were absent in that part of the assay. Given this observed

incoherence, an external study on particle behaviour was done to improve our understanding of these data and to avoid drawing erroneous conclusions from this image parameter.

The displacement of particle cumulus on glass was studied by the same image analysis to model how particle accumulation disintegrated by dragging at two lengths. Figure 7 shows an example of this study. The lefthand zone reveals a sequence of the real displacement studied in the greyscale images. Particle accumulation intensity was high (red line) with grey levels between 199 and 245. The colour profile shows the maximum intensity for the central accumulation zone given the large amount of particles (Figure 7A, central zone). The histogram of that accumulation shows high pixels frequency for that zone of intensities, which represents a large fraction of pixels from the total. Its displacement generated more particle accumulations with smaller sizes, which also showed less colour intensity (Figure 7B and 7C, central zone, green line). This means loss of material from the initial accumulation, but the area detected by the image analysis was bigger, as the histogram area shows. In addition, histograms increased the total area fraction because of the increased area for minor accumulations (green lines) and it reduced for the initial one (red lines). These results prove that the area of a given amount of particles can increase because of mass loss with movement phenomena while dragging across spaces. It allowed us to conclude that the absence of food for group-A modified drag dynamics and, thus, the disintegration of particle cumulus to detect a bigger area of particles.

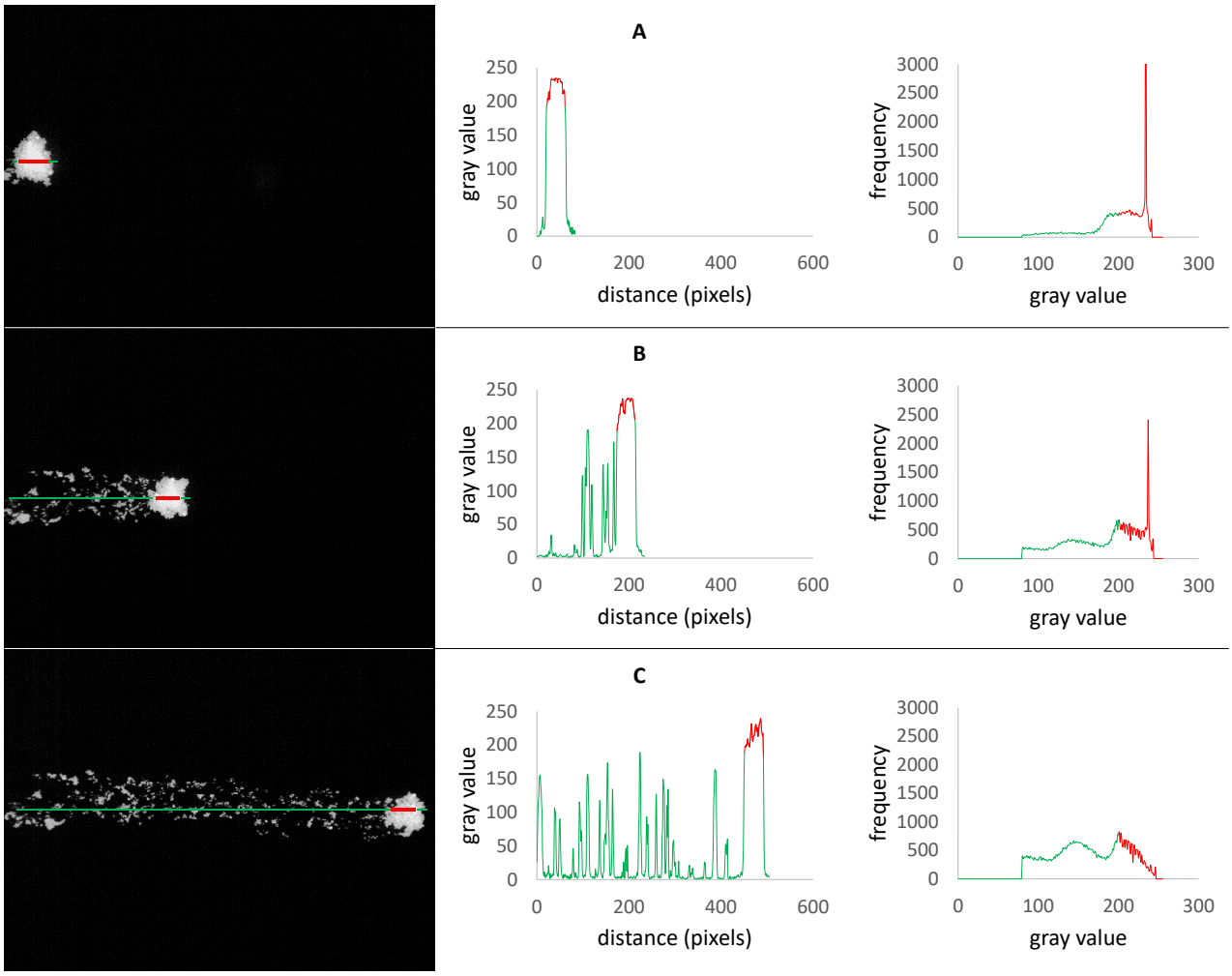

Figure 7. Study of particle aggregates broken on glass. Left: the grey scale image of the initial particles aggregate; centre: the colour profile on the grey scale; right: histogram of images. A: initial particle aggregates morphology; B: intermediate particle aggregates disaggregation; C: maximum disaggregates of particle aggregates.

Figure 8 illustrates an example of that phenomenon in nematodes, where two particle distributions from nematodes of both groups in the depuration phase (30 h) are compared. The processed images show the difference in distributions across nematodes. The group-P nematodes (Figure 8A) showed a shorter particle distribution; that is, a low *L* because of the close *A* and *B* values, as well as a low P_A due to the minimum disintegration of particle accumulations. Conversely, Figure 8B depicts a group-A nematode with an extended particle distribution and a higher P_A starting with the same amount of particles. The peaks obtained by the grey profile showed differences in particle aggregates. Particles produced greater intensity when they remained aggregated.

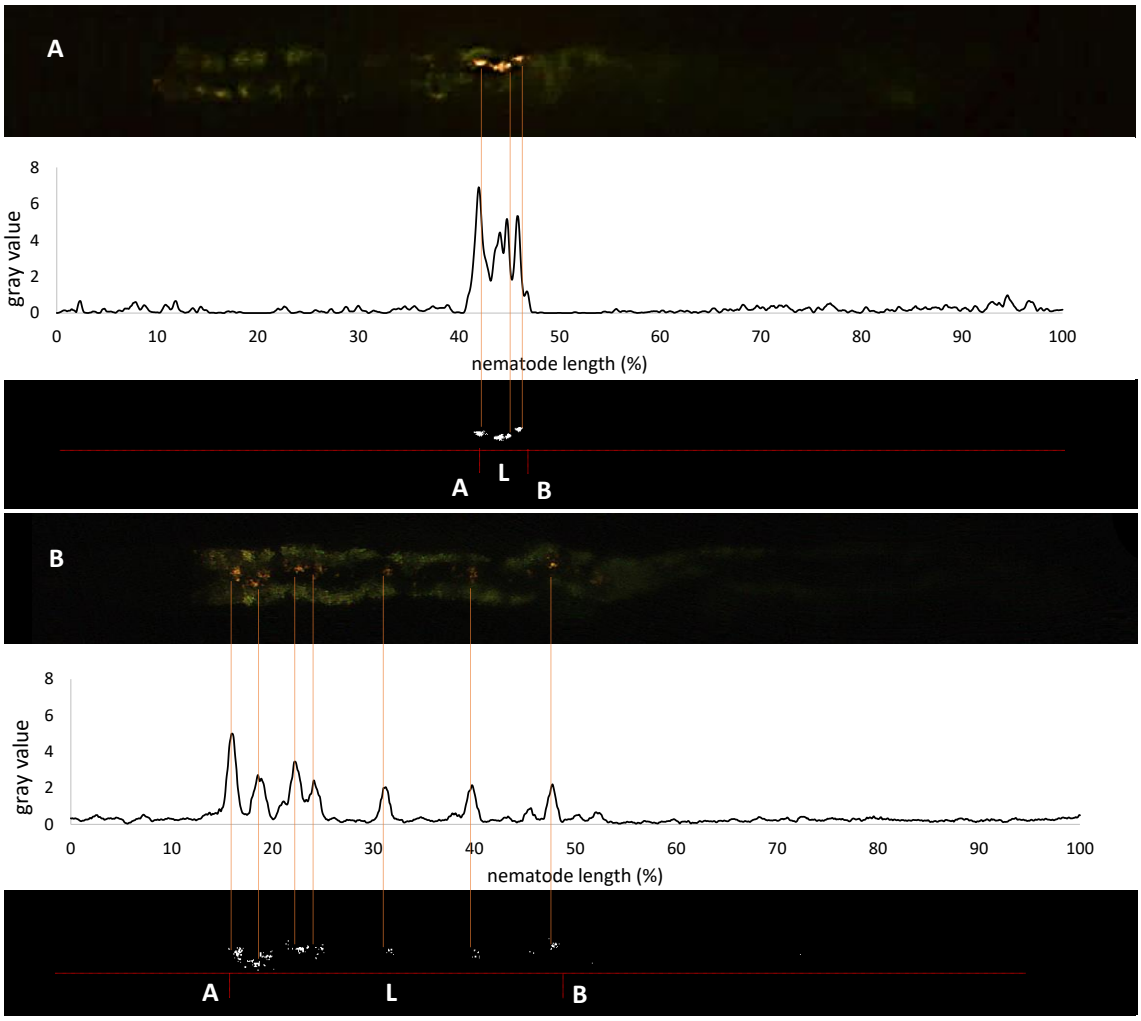

Figure 8. Study of particle distributions in nematodes at 30 h (depuration phase). A: fluorescence image of the MCM-particle distribution in the nematodes of group-P; B: fluorescence image of the MCM-particle distribution in the nematodes of group-A. Top: original fluorescence image; Intermediate zone: the grey profile of fluorescence images showing peaks due to fluctuations in colour produced by the detection of particles; Bottom: images of isolated particles after processing by image segmentation. The red line represents nematode length from the head to the end of particle distribution, where *A*: start of the MCM-particle distribution; *B*: end of the MCM-particle distribution; *L = B-A*.

Therefore, the area of particles was also related to the presence of food. The incorporation-excretion kinetics indicated major differences depending on food availability to maintain a flux of matter into the digestion system and synchronised excretion. The presence of particles stimulated their incorporation, but their progress slowed down once inside nematodes, which

produced extended distributions along digestive tubes which, in turn, generated different excretion velocities and then accumulation. Hence the changes observed at the beginning of the depuration phase could be divided into two main effects with the presence of food depending on the group. For group-A, increasing the particles area was due to the reduced stimulus, as mentioned above. For group-P, a reduced particles area meant increased excretion because of the permanent food stimulus (Figure 6, red arrows).

4. Conclusions

The influence of the presence of food on the incorporation and distribution kinetics of silica particles in *C.elegans* was significant. Incorporation of particles into the digestives tubes of nematodes took place both with and without food being present. This meant that the MCM-particles could pass to digestive tubes themselves without bacteria having to be present. No differences were observed for any parameter in the exposure phase, but an effect on the depuration phase was detected for both the distribution and excretion kinetics. Particles presented higher distributions in nematodes when no food was administered. That fact produced more particle aggregates due to the modification made to the movement kinetics because of reduced excretion stimulus. The increased residence time in the nematode body led to more particles being detected given the disintegration of particle aggregates, which led to more particle aggregates along digestive tubes. Therefore, the particles area was also related to the presence of food. The presence of particles stimulated their incorporation. However, their progress slowed down once inside nematodes, which led to extended distributions along digestive tubes which, in turn, generated different excretion velocities and then accumulation.

According to these results, intake of MCM-particles had no retention effects on nematodes when a food flux was provided, but particles were not easily excreted when the food flux was interrupted. This stresses the need to know what happens with particles that are stored because food is lacking, and to evaluate the plausible toxic effects from a chronic point of view.

5. Declaration of competing interest

The authors have no conflicts of interest to declare.

6. Acknowledgement

The authors gratefully acknowledge the financial support from the Universitat Politècnica de València by Programme "Ayudas para la Contratación de Doctores para el Acceso al Sistema Español de Ciencia, Tecnología e Innovación, en Estructuras de Investigación de la UPV (PAID-10-17)" and Ministerio de Ciencia, Innovación y Universidades, the Agencia Estatal de Investigación and FEDER-EU (Project RTI2018-101599-B-C21).

7. Bibliography

Ahn, J.M., Eom, H.J., Yang, X., Meyer, J.N., Choi, J., 2014. Comparative toxicity of silver nanoparticles on oxidative stress and DNA damage in the nematode, Caenorhabditis elegans. Chemosphere. https://doi.org/10.1016/j.chemosphere.2014.01.078

Altun, Z.F., Herndon, L.A., Norris, C., Xu, M., Crocker, C., Stephney, T., Hall, D.H., 2007. WormAtlas and WormImage: The Websites and the Book. Int. Worm Meet.

Arndt, D.A., Oostveen, E.K., Triplett, J., Allan Butterfield, D., Tsyusko, O. V., Collin, B., Starnes, D.L., Cai, J., Klein, J.B., Nass, R., Unrine, J.M., 2017. The role of charge in the toxicity of polymer-coated cerium oxide nanomaterials to Caenorhabditis elegans. Comp. Biochem. Physiol. Part - C Toxicol. Pharmacol. https://doi.org/10.1016/j.cbpc.2017.08.009

Breimann, L., Preusser, F., Preibisch, S., 2019. Light-microscopy methods in C. elegans research. Curr. Opin. Syst. Biol. https://doi.org/10.1016/j.coisb.2018.11.004

Brenner, S., 1974. The genetics of Caenorhabditis elegans. Genetics.

Cha, Y.J., Lee, J., Choi, S.S., 2012. Apoptosis-mediated in vivo toxicity of hydroxylated fullerene nanoparticles in soil nematode Caenorhabditis elegans. Chemosphere 87, 49–54. https://doi.org/10.1016/j.chemosphere.2011.11.054

Däwlätşina, G.I., Minullina, R.T., Fakhrullin, R.F., 2013. Microworms swallow the nanobait: The use of nanocoated microbial cells for the direct delivery of nanoparticles into Caenorhabditis elegans. Nanoscale. https://doi.org/10.1039/c3nr03905f

Donald L Riddle, 1997. C. elegans II. 2nd edition. Cold Spring Harb. Lab. Press.

Fuentes, C., Ruiz-Rico, M., Fuentes, A., Ruiz, M.J., Barat, J.M., 2020. Degradation of silica particles functionalised with essential oil components under simulated physiological conditions. J. Hazard. Mater. https://doi.org/10.1016/j.jhazmat.2020.123120

Gonzalez-Moragas, L., Berto, P., Vilches, C., Quidant, R., Kolovou, A., Santarella-Mellwig, R., Schwab, Y., Stürzenbaum, S., Roig, A., Laromaine, A., 2017a. In vivo testing of gold nanoparticles using the Caenorhabditis elegans model organism. Acta Biomater. https://doi.org/10.1016/j.actbio.2017.01.080

Gonzalez-Moragas, L., Roig, A., Laromaine, A., 2015. C. elegans as a tool for in vivo nanoparticle assessment. Adv. Colloid Interface Sci. 219, 10–26. https://doi.org/10.1016/j.cis.2015.02.001

Gonzalez-Moragas, L., Yu, S.M., Benseny-Cases, N., Stürzenbaum, S., Roig, A., Laromaine, A., 2017b. Toxicogenomics of iron oxide nanoparticles in the nematode C. elegans. Nanotoxicology. https://doi.org/10.1080/17435390.2017.1342011

Maurer-Jones, M.A., Gunsolus, I.L., Murphy, C.J., Haynes, C.L., 2013. Toxicity of engineered nanoparticles in the environment. Anal. Chem. https://doi.org/10.1021/ac303636s

Nowack, B., Bucheli, T.D., 2007. Occurrence, behavior and effects of nanoparticles in the environment. Environ. Pollut. https://doi.org/10.1016/j.envpol.2007.06.006

Pluskota, A., Horzowski, E., Bossinger, O., Von Mikecz, A., 2009. In Caenorhabditis elegans nanoparticle-bio-interactions become transparent: Silica-nanoparticles induce reproductive senescence. PLoS One. https://doi.org/10.1371/journal.pone.0006622

Ribes, S., Ruiz-Rico, M., Pérez-Esteve, É., Fuentes, A., Barat, J.M., 2019. Enhancing the antimicrobial activity of eugenol, carvacrol and vanillin immobilised on silica supports against Escherichia coli or Zygosaccharomyces rouxii in fruit juices by their binary combinations. LWT. https://doi.org/10.1016/j.lwt.2019.108326

Ruiz-Rico, M., Pérez-Esteve, É., Bernardos, A., Sancenón, F., Martínez-Máñez, R., Marcos, M.D., Barat, J.M., 2017. Enhanced antimicrobial activity of essential oil components immobilized on silica particles. Food Chem. 233. https://doi.org/10.1016/j.foodchem.2017.04.118

Ruszkiewicz, J.A., Pinkas, A., Miah, M.R., Weitz, R.L., Lawes, M.J.A., Akinyemi, A.J., Ijomone, O.M., Aschner, M., 2018. C. elegans as a model in developmental neurotoxicology. Toxicol. Appl. Pharmacol. https://doi.org/10.1016/j.taap.2018.03.016

Stiernagle, T., 2006. Maintenance of C. elegans. WormBook. https://doi.org/10.1895/wormbook.1.101.1

Turan, N.B., Erkan, H.S., Engin, G.O., Bilgili, M.S., 2019. Nanoparticles in the aquatic environment: Usage, properties, transformation and toxicity—A review. Process Saf. Environ. Prot. https://doi.org/10.1016/j.psep.2019.08.014

Verdú, S., Ruiz-Rico, M., Perez, A.J., Barat, J.M., Talens, P., Grau, R., 2020. Toxicological implications of amplifying the antibacterial activity of gallic acid by immobilisation on silica particles: A study on C. elegans. Environ. Toxicol. Pharmacol. https://doi.org/10.1016/j.etap.2020.103492

Zhou, D., Yang, J., Li, H., Cui, C., Yu, Y., Liu, Y., Lin, K., 2016. The chronic toxicity of bisphenol A to Caenorhabditis elegans after long-term exposure at environmentally relevant concentrations. Chemosphere 154, 546–551. https://doi.org/10.1016/j.chemosphere.2016.04.011